"Scarring" and suppression of ionization in very intense radiation fields

Bala Sundaram
Department of Physics and Astronomy, The Johns Hopkins University, Baltimore, Maryland 21218

R.V. Jensen*
Department of Physics, Wesleyan University, Middletown, Connecticut 06457
and Institute for Theoretical Atomic and Molecular Physics, Harvard-Smithsonian Center for Astrophysics, Cambridge, Massachusetts 02138
(Received 17 August 1992)

The interaction of a model atom with very intense radiation fields is well approximated by a map that describes a free particle being kicked periodically by a double-well potential. Both the classical and quantum versions of the map are studied and are shown to provide a compact description of high-field stabilization in this strongly perturbed quantum system. In particular, we find that the "stabilized" wave function results from the excitation of a superposition of eigenstates of the periodic, time-evolution operator that are localized near classically unstable and weakly stable orbits. These "scarred" wave functions correspond to localized wave packets that oscillate back and forth in the strong external field while in the neighborhood of the attractive Coulomb field. The periodic bremsstrahlung, emitted as this wave packet passes the nucleus, provides a distinct experimental signature of the stabilized state.

PACS number(s): 32.80.Rm, 05.45.+b, 42.50.Hz

I. INTRODUCTION

Atomic physics is currently experiencing a renaissance in the use of classical mechanics in the description of strongly perturbed and strongly coupled quantum systems [1, 2] where the traditional perturbative treatment of the Schrödinger equation breaks down. In particular, recent advances in classical nonlinear dynamics and chaos have had important applications in the description of the photoabsorption spectrum of Rydberg atoms in strong magnetic fields [3], the microwave ionization of highly excited hydrogen atoms [4], and the excitation of doubly excited states of helium atoms [5]. The purpose of this paper is to expand on the results of our earlier Comment [6] that showed how these new methods of classical nonlinear dynamics and "quantum chaos" can be successfully used to describe the remarkable phenomenon of "stabilization" of ground-state atoms in super-intense laser fields.

The development of very intense laser fields with intensities larger than 10^{19} W/cm^2 provides an opportunity to explore the properties of matter in strong electromagnetic fields that greatly exceed the Coulomb binding fields in an atom. Since the photoionization rates calculated using perturbation theory increase rapidly with increasing laser intensity, one might expect that atoms exposed to these fields would be rapidly ionized. However, in a preliminary numerical study of the quantum dynamics of a one-dimensional (1D) model atom in a very intense laser field, Su, Eberly, and Javanainen (SEJ) [7] found that the ionization probability actually decreases when the oscillating field strength becomes much greater than the Coulomb binding field.

In these numerical studies, SEJ [7] considered a 1D Hamiltonian of the form (in a.u.)

$$H(x,p,t) = p^2/2 - 1/\sqrt{1+x^2} + xF\cos(\omega t + \phi)\ , \qquad (1)$$

where F, ω, and ϕ are the field strength, frequency, and phase of the oscillating electric field. (This 1D model potential asymptotes to the Coulombic potential for large x, but eliminates the singular behavior at the origin.) The corresponding time-dependent Schrödinger equation was solved on a space-time grid and the ionization probability computed by projecting out the continuum component of the time-dependent solution. As the perturbing field was increased from $F = 1.0$ to 5.0 a.u. the ionization probability for interaction times of approximately 30 field cycles decreased dramatically. In addition, their graphs of the electron probability as a function of position x indicated that this high-field stabilization of the atom was due to the localization of the electron probability to a double-peak structure which they associated with the "dichotomous" wave function in the time-averaged atomic potential studied by Pont *et al.* [8]. However, the peaks of the dichotomous wave functions were predicted [8] to be separated by a distance $2F/\omega^2$ while SEJ's peaks were only F/ω^2 apart.

In our earlier Comment [6] we briefly indicated how many features of these 1D simulations could be *correctly* accounted for using a synthesis of ideas and techniques for the classical, semiclassical, and quantum description of this strongly perturbed system. By approximating the classical equations of motion in the oscillating Kramers-Henneberger (KH) frame [9] by a nonlinear, area-preserving map, we showed that the classical electron dynamics undergoes a transition from chaotic, unstable, rapidly ionizing behavior for perturb-

ing fields comparable to the atomic binding fields, to stable, bounded motion as the fields are increased. Moreover, by diagonalizing the quantum-mechanical time-evolution operator corresponding to this classical map, we found that some of the *quasienergy* (QE) states, that describe the quantum dynamics of this periodically perturbed system, remain highly localized to the vicinity of classical periodic orbits even when the classical dynamics is fully chaotic and these periodic orbits are unstable. In particular, for the parameters of SEJ's simulations we suggested that if a *superposition* of these "scarred" [6] QE states are *diabatically* excited by the rapid turn-on of the applied field, then the resulting electron probability distribution could remain localized to the vicinity of the nucleus with peaks spaced F/ω^2 apart.

In this paper we develop further the classical, semiclassical and quantum analyses of the electron dynamics of 1D models of atoms in very strong fields, and we elaborate on our earlier results. We begin in Secs. II and III by providing a detailed discussion of our earlier demonstration [6] that the classical dynamics is well approximated by an impulsive map which describes the position and momentum of the classical particle once every external period.

This map facilitates the evaluation of the stability of the classical dynamics and the computation of the invariant structures [10] (fixed points, periodic orbits, KAM tori, stable and unstable manifolds, etc.) that partition the classical phase space. These structures, in turn, provide the "support" for quantum states and determine both the extent of stabilization as well as the structure of the residual wave function. The analysis of the structure and stability of the classical phase space for our nonlinear map is presented in Sec. IV. We find that the stability of the classical dynamics is determined by two key parameters. The first is the maximum excursion of the electron in the oscillating electric field,

$$\alpha = F/\omega^2 , \tag{2}$$

which must be large for the map approximation to the continuous classical dynamics to be valid. The second parameter is the "stochasticity parameter,"

$$S \approx 1/\sqrt{F}\omega , \tag{3}$$

which determines the stability of the classical dynamics. When S is large the classical electron motion in the vicinity of the nucleus is chaotic and rapidly leads to ionization.

Although the importance of α has been recognized by many others [7, 8, 11–15] the stochasticity parameter S, which decreases both with increasing field and frequency, is new. The combination of these requirements leads to an explicit condition for the onset of classical stabilization in this 1D model. In particular, the classical theory for this 1D model predicts that stabilization is not simply a high-frequency phenomenon but can occur even at low frequencies ($\omega \ll 1$) as long as $F > 1/\omega^2$.

In periodically driven systems, the eigenstates of the single-cycle evolution operator provide a compact description of the quantum dynamics. The quantized version of the classical map, in turn, gives us an approximation to this propagator which is easily diagonalized within a plane-wave basis. The resulting eigenvectors or QE states are closely linked to the structure of classical phase space. We show in Sec. V that the multiply peaked residual wave functions in the numerical simulations result from the *diabatic* excitation of eigenvectors that are highly localized in the vicinity of unstable and weakly stable periodic orbits embedded in the classically chaotic phase space. These highly structured wave functions associated with periodic orbits in a classically chaotic system are called "scars" [16]. The superposition of eigenvectors that result in the stabilized wave functions correspond to localized wave packets that oscillate back and forth in the strong external field but remain localized in the neighborhood of the attractive Coulomb field.

In Sec. VI we examine the possible experimental implications with particular emphasis on the odd and *even* harmonic generation arising from periodic bremsstrahlung as the wave packet passes the nucleus. This experimental signature of the stabilized state has also been observed in the three-dimensional (3D) numerical simulations of Kulander, Schafer, and Krause [15]. In the course of this discussion, we contrast both the power in the higher harmonics and their intensity dependence with the low-field harmonic generation profiles which were studied earlier [17]. Details of the classical derivations and a summary of the methodology used for the quantum dynamics are included in Appendixes A and B.

However, before beginning this detailed program, we find it necessary to dispell some points of confusion in the literature: (1) over various models of "stabilization", (2) on the applicability of classical mechanics to this quantum problem, and (3) on the role of the KH transformation.

A. Definition of "stabilization"

Although a variety of different theories and physical mechanisms have been proposed for the stabilization of atoms in intense, high-frequency fields [6–8, 12–15, 18], these can be roughly divided into two categories. The first class relies on the excitation of a quantum wave packet that maintains a small overlap with the nucleus. Since the absorption of energy in high-frequency fields can occur only near the nucleus, the ionization of these special wave packets can be greatly suppressed. Extreme fields and frequencies are not necessarily required to achieve this stabilization of weakly interacting wave packets, only some theoretical [12, 13, 18] or (very recently) experimental ingenuity [19]. Moreover, in many of these models "stabilization" refers to a saturation of the ionization rate with increasing fields rather than to a decrease in the ionization probability.

A second, more dramatic mechanism for atomic stabilization in intense, high-frequency fields is illustrated in the numerical simulations by SEJ for 1D model atoms and by Kulander, Schafer, and Krause [15] for $m = 0$ states of 3D hydrogen atoms. In these calculations the

ionization probability first increases with increasing field as expected by perturbation theory and then exhibits a sharp decrease when the perturbing field strengths exceed the magnitude of the typical atomic binding fields. In contrast with the first weakly interacting mechanism for the suppression of ionization, this stabilization mechanism depends on the *strong* interaction with the atomic nucleus since the electron wave packet in the oscillating field alone would rapidly spread apart. As the Kramers-Henneberger transformation is important for the prediction and description of this effect, we will refer to this strongly interacting stabilization mechanism as KH stabilization.

B. Applicability of classical mechanics

The principal aim of this paper is to thoroughly explore the classical and semiclassical description of KH stabilization in the one-dimensional model system introduced by SEJ. One justification for the application of classical mechanics to this quantum problem is the observation that in strong fields, when $\alpha \gg 1$, the perturbed electron dynamics may extend over many atomic units of distance, coupling many zero-field atomic states. In this case the high density of coupled states greatly complicates the quantum theory, but this is precisely the situation where a classical theory may be most effective (at least for the short times of the radiation pulse). Although the utility of the classical description of the strongly perturbed electron dynamics has also been recognized by several other groups [20–22], this approach has also been subject to some criticism. However, the failures of other classical analyses of this problem can be largely attributed to incorrect or incomplete treatments of the classical mechanics and of the classical-quantum correspondence for these strongly perturbed systems.

For example, based on a limited sample of 1D and 3D classical simulations of the atomic electron dynamics in strong oscillating fields, Grochmalicki, Lewenstein, and Rzazewski [21] conclude that the classical dynamics exhibits stabilization in the 1D but not the 3D models and that, consequently, the stabilization observed in SEJ's quantum 1D simulations would not survive in a more realistic 3D quantum calculation. However, this prediction based on the classical simulations was promptly disproved by the 3D quantum simulations of hydrogen atoms by Kulander, Schafer, and Krause [15] which clearly exhibited KH stabilization and also by two-dimensional simulations of a model potential by You, Mostowski, and Cooper [22].

Does this failure imply that classical mechanics is not applicable to this problem? The answer is an emphatic no, as shown by the results of our detailed analysis of the classical nonlinear dynamics in Sec. IV. For the field parameters studied in the 1D simulations of Grochmalicki, Lewenstein, and Rzazewski [21], the classical dynamics in the vicinity of the nucleus becomes completely stable. Many classical electron orbits starting near the nucleus never ionize. In the classical theory this stabilization arises because the perturbing field becomes much larger than the binding field of the atom which can then be treated as a small perturbation on the regular, integrable motion in the oscillating field alone.

In contrast, the classical dynamics for all of the $m = 0$ orbits in the 3D hydrogen atom appear to remain highly unstable and chaotic in large fields, as the oscillating field can never dominate the bare Coulomb singularity. A more appropriate 1D case to compare with 3D simulations would be the original parameters chosen by SEJ [7]. In this example we find that (except for a very small set of initial conditions) the 1D classical dynamics is also completely unstable and chaotic, like the generic, $m = 0$, case in 3D. In these situations, recent developments in the quantum description of classically chaotic systems suggest that quantum states may still remain localized in so-called "scarred" states that are associated with unstable periodic orbits.

In Sec. V we construct these scarred quantum states for SEJ's parameters and demonstrate how the proper interpretation of the classical-quantum correspondence for this classically chaotic system successfully describes the quantum 1D simulations. From this agreement we suggest that the stabilization observed by Kulander, Schafer, and Krause [15] in 3D is also due to the excitation of a superposition of scarred quasienergy wave functions. Although the quantum dynamics may be very different from the classical dynamics, a detailed understanding of the structure of the classical space for this strongly perturbed system can nevertheless prove to be very useful in understanding the structure of the stabilized wave functions.

C. Role of KH states

A common explanation for KH stabilization is to argue that in high-frequency fields the electron only sees an effective, time-averaged potential. On Fourier transforming the potential in the oscillating KH frame, the time-dependent parts of the potential can be separated from the time-averaged piece and treated as small perturbations [8]. The bound eigenstates, called KH states, of the effective time-independent Hamiltonian are stable by definition. As a consequence, many authors talk about the excitation of KH states in strong, high-frequency fields.

However, this terminology can lead to some confusion since the original time-periodic dynamical system cannot be so easily replaced by a time-independent problem. In particular, we show in Secs. III and IV that the time-dependent contributions in the Fourier expansion of oscillating potential can be comparable to the time-independent piece. Consequently, in our map approximation for the classical and quantum dynamics in the oscillating field we treat all terms in the Fourier expansion as equal in importance.

It is important to recognize that, in the presence of a periodic radiation field, a superposition of Floquet, QE states is excited. These time-dependent states are not the same as the time-independent KH states. However, we demonstrate in Sec. V that for wide ranges of parameters, the structure of these QE states, viewed once every period of the perturbation, can be very similar to the

eigenfunctions of the time-averaged potential. In these cases, the stabilized QE wave functions can be said to *resemble* the KH states.

When the classical dynamics is regular in the 1D model as for small values of the stochasticity parameter S this connection between the QE states and the KH states can be more firmly established using traditional semiclassical methods. However, when the classical motion is chaotic but the quantum evolution remains stable (for $S \sim 1$), the most stable QE states correspond to scarred states. In the latter case the persistent resemblance of these two very different types of wave functions is quite remarkable and is an outstanding problem for future research [23].

II. CLASSICAL DYNAMICS

In the high-field limit ($F \gg 1$ a.u.) the smoothed Coulomb potential in Eq. (1) can be treated as a perturbation on the regular, classical motion of a free electron in an oscillating field. So, we first consider the Hamiltonian for the one-dimensional motion of a free electron in the oscillating electric field $E = F\cos(\omega t + \phi)$,

$$H_0(x,v,t) = v^2/2 - xF\cos(\omega t + \phi)\ . \tag{4}$$

The classical equations of motion can be integrated exactly and the solution for the position of the electron as a function of time,

$$x(t) = x_0 - \frac{F}{\omega^2}[\cos(\omega t + \phi) - \cos\phi] + \left[v_0 - \frac{F}{\omega}\sin\phi\right]t\ , \tag{5}$$

describes a particle that oscillates back and forth in the electric field with frequency $\nu = \omega/2\pi$ and amplitude α and drifts away from its initial position x_0 with velocity

$$v_d = v_0 - \frac{F}{\omega}\sin\phi\ . \tag{6}$$

[Note that even if the initial velocity v_0 is zero, a nonzero initial phase ϕ of the oscillating field can lead to a large drift velocity, $v_d = -(F/\omega)\sin\phi$.]

The classical motion is considerably simplified if we perform a canonical change of variables to the oscillating frame

$$\begin{aligned} q &= x + \alpha[\cos(\omega t + \phi) - \cos\phi], \\ p &= v - \left[\frac{F}{\omega}\sin(\omega t + \phi)\right]. \end{aligned} \tag{7}$$

In the absence of any other forces $p = v_d$ is constant and the oscillation center drifts at the constant velocity $q(t) = x(0) + v_d t$. In particular, if $v_d = 0$ (e.g., $v_0 = 0$ and $\phi = 0$ or π), then $q(t) = x_0$ is constant.

The introduction of a perturbing potential $V(x)$ will alter the free motion of the oscillation center q. In the oscillating frame $V(x)$ appears as a time-dependent potential in the transformed Hamiltonian

$$H(q,p,t) = p^2/2 + V(q - \alpha[\cos(\omega t + \phi) - \cos\phi])\ , \tag{8}$$

which can be conveniently expanded in a discrete Fourier series

$$H(q,p,t) = p^2/2 + \sum_{n=-\infty}^{\infty} V_n(q)e^{in\omega t}\ , \tag{9}$$

as the perturbation is periodic with period $T = 2\pi/\omega$. The Fourier coefficients are

$$V_n(q) = \frac{1}{T}\int_0^T V(q - \alpha[\cos(\omega t + \phi) - \cos\phi])e^{-in\omega t}dt, \tag{10}$$

where

$$V_0(q) = \frac{1}{T}\int_0^T V(q - \alpha[\cos(\omega t + \phi) - \cos\phi])dt \tag{11}$$

is simply the time average of the oscillating potential. It is this time-averaged component that is often referred to as the KH potential.

In general, the effects of the perturbation can only be assessed by numerically integrating the Hamiltonian equations of motion generated by Eqs. (10) or (11). However, if the perturbing potential is not too singular and has a limited effective range r, which is much less than the excursion of the oscillating electron α, then the electron receives the largest impulse from the potential during the short time when the oscillating electron is moving slowly as it reverses its direction on the side closest to the perturbing potential [24].

This can also be seen mathematically if we express the Fourier coefficients of the $V(x(t))$ as integrals over x,

$$\begin{aligned} V_n(q) &= \frac{1}{T}\int_0^T V(x(t))e^{-in\omega t}dt \\ &= \frac{1}{T}\int V(x)\frac{e^{-in\omega t(x)}}{v(x)}dx\ , \end{aligned} \tag{12}$$

where the velocity of the oscillating electron, for fixed q

$$v(x) = \frac{F}{\omega}\sin(\omega t + \phi) = \frac{F}{\omega}\sqrt{1 - [(x-q)/\alpha + \cos\phi]^2}\ , \tag{13}$$

goes to zero at the turning points $x^{\pm} = \pm\alpha - \alpha\cos\phi + q$. Moreover, as the range of the potential is much less than α, the contribution from one of the turning points will always be greater than the other. The exception is when the oscillating orbit is centered on the potential, but in this case the contributions from both turning points will be relatively small.

Therefore when $\alpha \gg r$, we find that the classical equations of motion in the oscillating, Kramers-Henneberger frame are well approximated by assuming the electron experiences an impulsive "kick" once every period of the oscillation, $T = 2\pi/\omega$. Then the classical differential equations of motion can be replaced by a pair of differ-

ence equations that define a nonlinear, area-preserving map,

$$q_{n+1} = q_n + Tp_{n+1},$$
$$p_{n+1} = p_n + G(q_n), \tag{14}$$

where q_n and p_n are the positions and momenta of the electron in the oscillating KH frame, evaluated once every period $T = 2\pi/\omega$ of the field. The total impulse of each kick $G(q_n)$ is the time integral of the force over one period of an unperturbed oscillation with $q(0) = q_n$ and $p(0) = 0$ which can be simply expressed in terms of the space derivative of the time integral of the oscillating potential,

$$G(q_n) = -\frac{d}{dq} TV_0(q)|_{q=q_n} . \tag{15}$$

This physically motivated derivation of our nonlinear map, Eq. (14), is equivalent to simply approximating all of the Fourier coefficients, $V_n(q)$, in Eq. (9) by $V_0(q)e^{in\omega\phi}$. Then the Hamiltonian in the oscillating frame reduces to

$$H(q,p,t) \approx p^2/2 + V_0(q) \sum_{n=-\infty}^{\infty} e^{in\omega t} e^{in\omega\phi}$$
$$= p^2/2 + V_0(q) \sum_{n=-\infty}^{\infty} \delta(t - nT + \phi T/2\pi) , \tag{16}$$

using the Poisson sum rule. Since the phase of the perturbation simply determines the timing of the kicks, we will henceforth choose $\phi = 0$ with no loss of generality. [This choice of phase was motivated by the desire to avoid any unneccesary complications associated with the induced classical drift motion in Eq. (6) for $\phi \neq 0$ or π.] Finally, integrating the equations of motion for this kicked Hamiltonian with $\phi = 0$ over a single period leads to the map defined by Eq. (14).

A mathematical justification for our assumption that the Fourier coefficients are equal can be provided by expanding the integrand in Eq. (12) near the turning points. For example, when the electron experiences the largest interaction with the nucleus on the left side of its oscillating motion in the external field, then we can expand Eq. (10) about the right turning point $x = x^+ + \epsilon$, to get

$$V_n(q = x^+) \approx \frac{1}{T} \int \frac{V(x^+ \pm \epsilon) e^{-in(\sqrt{2\epsilon/\alpha})}}{\sqrt{1 - [1 - \epsilon/\alpha]^2} d\epsilon}. \tag{17}$$

Given the limited, effective range r of the perturbing potential the main contribution to the integral arises for $\epsilon \ll \alpha$. Then as long as $\epsilon_{\max} \approx r \ll \alpha/2n^2$ we can neglect the exponential phase in Eq. (17) to conclude that $V_n(q) \approx V_0(q)$ for $n \ll \sqrt{\alpha/2r}$. When $\alpha \gg r$, this condition will be satisfied for a number of Fourier components [25].

The validity of the map approximation for the classical dynamics of an electron interacting with a strong, oscillating field and a restricted range potential can also be checked *a posteriori* either by comparing the map dynamics with the solution of the full differential equations generated by Eq. (10) or by explicitly checking the assumption that the Fourier coefficients $V_n(q)$ are approximately equal to $V_0(q)$ for a wide range of n.

III. THE CLASSICAL MAP FOR A SMOOTHED COULOMB POTENTIAL

Let us now illustrate the arguments of Sec. II when the perturbation of the free, oscillatory motion of the electron is due to a smoothed Coulomb potential

$$V(x) = -Z/\sqrt{a^2 + x^2} , \tag{18}$$

where Z is the nuclear charge and a is a smoothing parameter that eliminates the x^{-1} singularity at the origin and also defines a characteristic length scale. In the oscillating KH frame with $\phi = 0$, this potential transforms to

$$V(q,t) = -Z/\sqrt{a^2 + (q - \alpha[\cos\omega t - 1])^2} . \tag{19}$$

(In SEJ's original studies [7] a was set to 1 a.u. of length and ϕ was chosen to be $\pi/2$.)

The time average of $V(q,t)$ can be evaluated exactly in terms of complete elliptic integrals. We defer the explicit derivation to Appendix A and use instead an analogy with the full Coulomb potential. As the time average of the smoothed Coulomb potential, Eq. (18), is identical to the time average of the three-dimensional Coulomb potential in cylindrical coordinates (ρ, x)

$$V(x,y) = -Z/\sqrt{x^2 + \rho^2}$$

with $|\rho| \equiv a$, we can simply take the previous result of Pont *et al.* [Eq. (5) of Ref. [8]]

$$V_0(q) = -(2Z/\pi)(r_+ r_-)^{-1/2} K(2^{-1/2}(1 - \hat{\mathbf{r}}_+ \hat{\mathbf{r}}_-)^{1/2}), \tag{20}$$

where K is the complete elliptic integral of the first kind. If we shift the origin to the oscillation center at $-\alpha$ of the free motion defined by Eq. (5), then $\mathbf{r}_+ = q\hat{\mathbf{x}} + a\hat{\mathbf{y}}$ and $\mathbf{r}_- = (q + 2\alpha)\mathbf{x} + a\hat{\mathbf{y}}$.

As shown in Fig. 1, the time-averaged potential in the oscillating KH frame, $V_0(q)$, for SEJ's field parameters of $F = 5.0$ (a.u.) and $\omega = 0.52$ a.u. is a double-welled potential with minima *near* the classical turning points for the free electron in the oscillating field at 0 and -2α. For the smoothed Coulomb potential the effective range r is set by the scale parameter a. Consequently, when $\alpha \gg a$ we can expand the time-averaged potential near the turning point close to $q = 0$

$$V_0^+(q) \approx -\frac{2\sqrt{2}}{T\sqrt{F}} \frac{Z}{(a^2 + q^2)^{1/4}} K(k_+^2) \tag{21}$$

with $k_+^2 = \frac{1}{2}(1 - q/\sqrt{a^2 + q^2})$. Similarly near the turning point close to $q = -2\alpha$,

$$V_0^-(q) \approx -\frac{2\sqrt{2}}{T\sqrt{F}} \frac{Z}{[a^2 + (q + 2\alpha)^2]^{1/4}} K(k_-^2), \tag{22}$$

where $k_-^2 = \frac{1}{2}[1+(q+2\alpha)/\sqrt{a^2+(q+2\alpha)^2}]$. By adding these two contributions together we get an approximate expression for the double-well potential $V_0(q) \approx V_0^+(q) + V_0^-(q) + \text{const}$ which is compared with the exact expression in Fig. 1, for the SEJ parameter values.

Using the approximate expressions for the kicking potential in the vicinity of the turning points we can derive an analytic formula for the kicking force

$$G(q) = -\frac{2\sqrt{2}Z}{\sqrt{F}}\{[E(k_+) - 0.5K(k_+)]/(a^2+q^2)^{\frac{3}{4}} - [E(k_-) - 0.5K(k_-)]/[a^2+(q+2\alpha)^2]^{\frac{3}{4}}\} \tag{23}$$

in terms of complete elliptic integrals of the first and second kind with arguments $k_\pm$ defined above. For completeness, an explicit derivation of the time-averaged potential (in 1D) as well as the approximate kicking force are included in Appendix A [26].

Finally, the approximation of the classical dynamics by a map requires that $V_n(q)$ be approximately equal to $V_0(q)$ for a range of n values. We show a direct confirmation of the validity of the assumption over a wide range of q for $n = 1, 2$ and for the SEJ parameter values in Fig. 2(a) as well as for field parameters giving $\alpha = 100$ in Fig. 2(b). The relative importance of the higher Fourier weights increases with increasing α but it is already clear from Fig. 2 that more than the time-averaged component $V_0(q)$ must be included to describe the dynamics for $\alpha > a$.

More generally, the validity of this approximation can be checked *a posteriori* by comparing the magnitude of the impulses experienced by the electron after each period of the oscillating field with those predicted for the map, Eq. (14). Figure 3 contrasts the impulse delivered over each cycle of the external field by the full differential dynamics with the single-valued function in Eq. (23), for four different values of α spanning a large range. It is

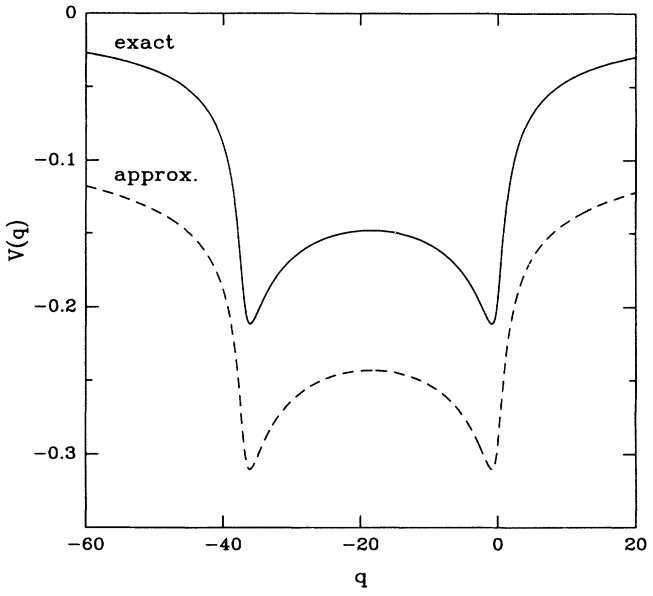

FIG. 1. Kick potential as a function of q for $F = 5.0$ (a.u.) and $\omega = 0.52$ (a.u.), for both exact and approximate (evaluated only in the vicinity of the classical turning points) kicking terms. The curves clearly show that a simple constant shift is the only difference.

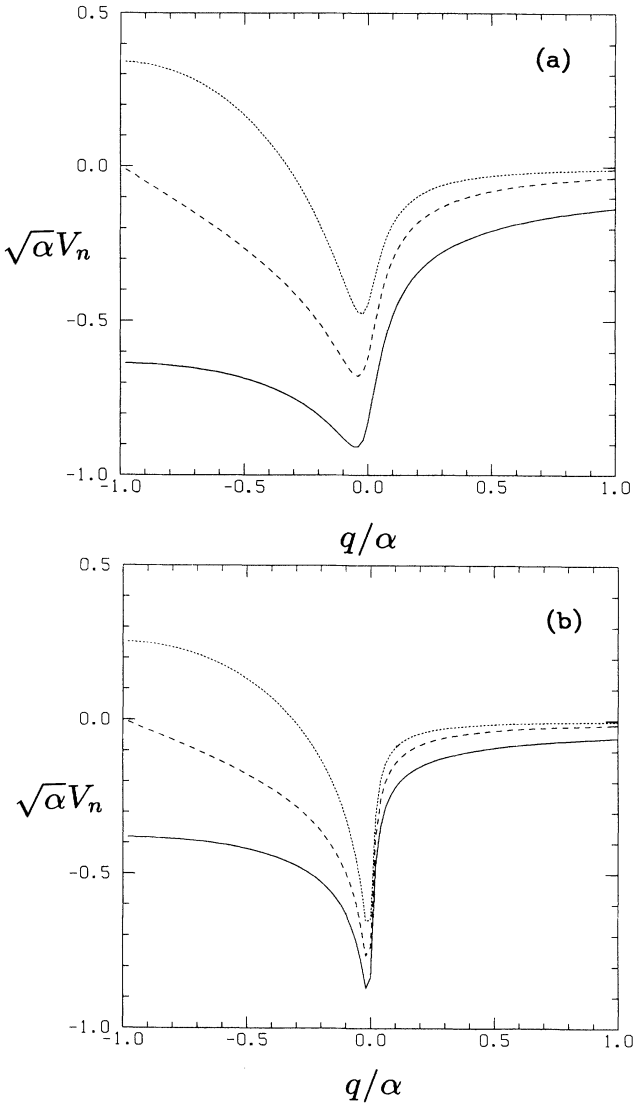

FIG. 2. Variation of the three lowest Fourier weights ($V_{0,1,2}$, from top to bottom) of the time-dependent potential in the KH frame, as a function of the position q. The field parameters correspond to α values of (a) 18.5 and (b) 100. Note that the quantities relevant to the dynamics are the gradients $dV_n(q)/dq$ which are seen to be very similar for $n = 0, 1, 2$ in both cases.

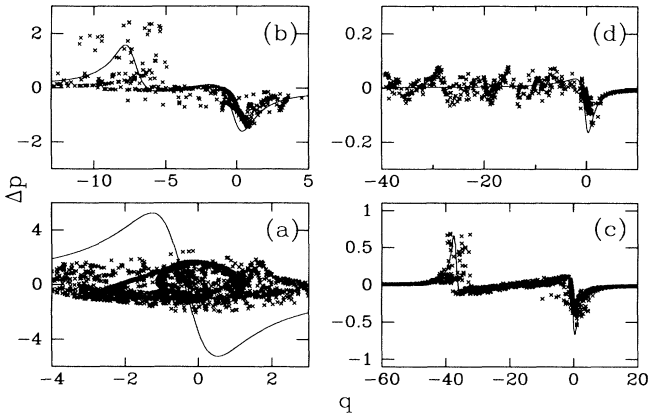

FIG. 3. Comparison of the impulse generated over a single period from the differential dynamics (crosses) and the single valued function [Eq. (23)] for the map. The parameter α is (a) 0.37, (b) 3.7, (c) 18.5, and (d) 295.9. (d) displays only a small portion of the total range so as to emphasize the maximum discrepancy.

clear from Fig. 3 that with increasing α, Eq. (23) is a very good approximation to the true impulse felt by the electron over each period of the oscillating field [27].

IV. CLASSICAL MAP DYNAMICS, FIXED POINTS, STABILITY, AND CHAOS

Having established the map as a good approximation to the true classical dynamics, we will now proceed with a general analysis of the stability of trajectories in the classical phase space. By iterating the map for a variety of initial conditions and plotting the trajectories in the two-dimensional (q_n, p_n) phase space, we can construct a Poincaré surface of section which provides an overview of the classical dynamics. For example, Fig. 4 shows the surface of section for the SEJ field parameters. Almost all of the classical electron orbits that start out near the nucleus are chaotic and ionizing. In contrast Fig. 5 shows the corresponding surface of section for the parameters used in Ref. [21]. In this case many initial conditions starting out near the nucleus are regular and remain bound, tracing out regular island structures in the classical phase space [28].

The global stability and instability of the classical phase space illustrated in Figs. 4 and 5 can be characterized by the stability of a special set of points in the phase space (q^*, p^*) which are mapped into themselves under the action of the map, $q_{n+1} = q_n = q^*$ and $p_{n+1} = p_n = p^*$. By linearizing the map about each of these *fixed points* we can analyze the local stability of the classical trajectories.

For the map defined by (14) there are, in general, three fixed points for $\alpha > 1$. All three have $p^* = 0$ with q^* given by the solutions of the transcendental equation $G(q^*) = 0$. One of these solutions is always at $q^* = -\alpha$, on the saddle point of the kicking potential V_0, while the other two lie in the minima of V_0 near $q = -2\alpha$ and 0.

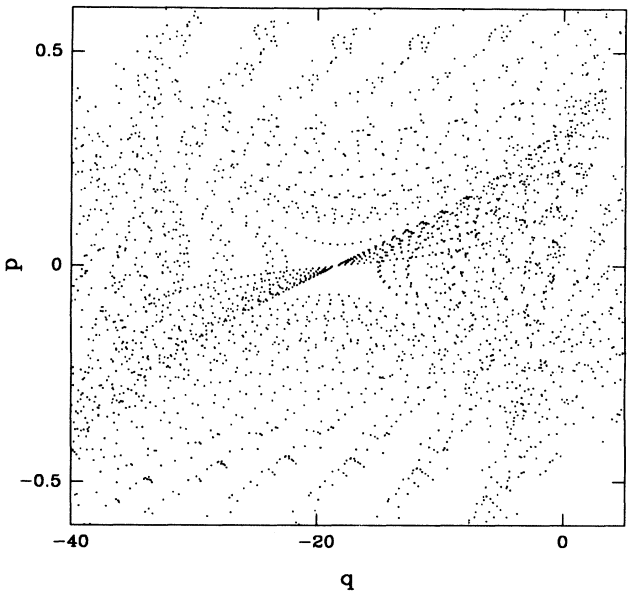

FIG. 4. Poincaré section for $F = 5.0$ and $\omega = 0.52$ which is typical for large values of the stochasticity parameter. As discussed in the text, no stable (island) structures are expected and the classical dynamics is dominated by rapidly ionizing orbits.

The linear stability analysis of the fixed points is based on the Jacobian matrix of the map given by

$$J = \begin{pmatrix} 1 + T\frac{dG(q)}{dq} & T \\ \frac{dG(q)}{dq} & 1 \end{pmatrix}, \tag{24}$$

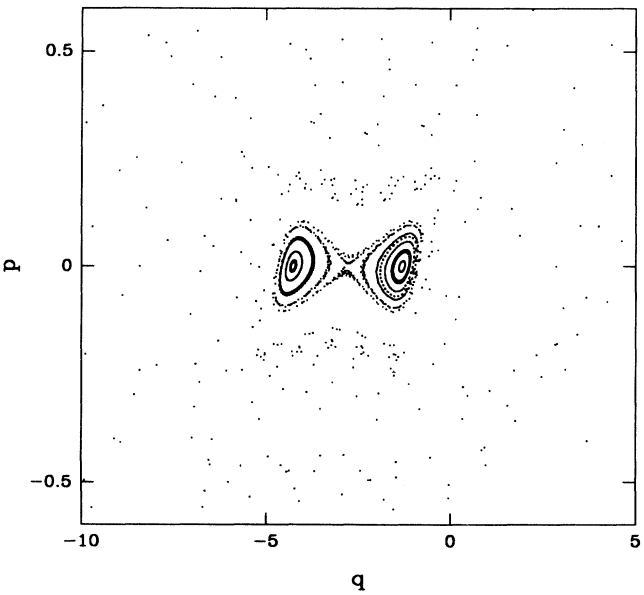

FIG. 5. Poincaré section for the "half-photon" ionization parameters $\omega = 1.34, F = 5.0$ of Ref. [21] showing the presence of stable classical islands. The occurrence of these stable regions is typical for small values of the stochasticity parameter.

where $T = 2\pi/\omega$ and $-dG(q)/dq = d^2V_0(q)/dq^2$ is the local curvature of the kicking potential. The symplectic or area-preserving character of the map is evident as $\det(J) = 1$ while the eigenvalues are

$$\lambda_\pm = \frac{(2+S) \pm \sqrt{S(S+4)}}{2} \tag{25}$$

with $S = T\frac{dG}{dq}$.

When $S|_{(q^*,p^*)} < -4$, both eigenvalues are real and negative, the fixed point is unstable and called *hyperbolic with reflection.* When $-4 < S|_{(q^*,p^*)} < 0$, the eigenvalues are complex and the fixed point is a stable, *elliptic* point. While for $S|_{(q^*,p^*)} > 0$ the eigenvalues are real and positive and the fixed point is an unstable, *hyperbolic* point. Thus, the changing character of the fixed points which govern the nature of the classical phase space can be determined by the magnitude and sign of S.

In the case of the smoothed Coulomb potential, there is first a regime where $\alpha = F/\omega < 1$ and V_0 is a single well with minimum at $-\alpha$. In this case all three fixed points coalesce at $q^* = -\alpha$ and $S_0 = S|(-\alpha, 0) < 0$ because the curvature of V_0 is positive. As the field strength F is increased at fixed frequency, the fixed point at $(-\alpha, 0)$ changes (as shown above) from hyperbolic with reflection (or an orientation reversing saddle) to elliptic on increasing F. Further increase to $\alpha > 1$ leads to the general case of three distinct fixed points where either (i) the primary fixed point at $(-\alpha, 0)$ is hyperbolic while the secondary fixed points near $(0, 0)$ and $(-2\alpha, 0)$ remain stable and elliptic as in Fig. 5 or (ii) all three are hyperbolic with no stable structures in the classical phase space as in Fig. 4.

For $\alpha > 1$ the primary fixed point $(-\alpha, 0)$ on the saddle between the double wells of V_0 is always unstable with $S_0 > 0$ because the local curvature of V_0 at this point is negative. Therefore, the global stability of the classical dynamics is controlled by the stability of the secondary fixed points. Because of the symmetry of the map we need only focus attention on the secondary fixed point, $(q_1, 0)$ near $(0, 0)$. To assess its stability, we must first determine its precise location, q_1, and then evaluate the curvature of the map potential at this point, $S_1 = -T^2 d^2V_0/dq^2|_{(q_1,0)}$. In practice the secondary fixed points and their stability can only be determined numerically; however, this analysis can be greatly simplified by approximating the map potential in the limit $\alpha \gg 1$ by

$$V_0^+(q) \approx -\frac{2\sqrt{2}Z}{T\sqrt{aF}} \frac{1}{(1+x^2)^{1/4}} K(k_+^2), \tag{26}$$

where $x \equiv q/a$ and $k_+^2 = \frac{1}{2}(1 - x/\sqrt{1+x^2})$. Numerical differentiation of Eq. (26) with respect to x indicates that the fixed point (where $dV_0/dx = 0$) is approximately equal to $q_1/a = 0.8$ and the stability parameter at this point is approximately determined by

$$S_1 \approx -2\pi Z/\sqrt{F}\omega a^{5/2} . \tag{27}$$

For the SEJ case with $Z = 1$ and $a = 1$, Eq. (27) reduces to our earlier prediction for the stochasticity parameter that determines the relative stability of the classical dynamics. For large fields F and frequency ω, so that $-4 < S_1 < 0$, the secondary fixed points are stable elliptic points surrounded by stable island structures in the classical phase space as shown in Fig. 5, which corresponds to field parameters giving $S_1 = -2.1$. However, when $S_1 < -4$ both the primary and secondary fixed points are unstable and the global classical dynamics tends to be unstable. This is the case for the SEJ field parameters where $S_1 = -5.4$, which lies beyond the boundary of stability predicted by Eq. (27) [29].

The scaling properties of Eq. (27) with respect to the shielding parameter a also clearly illustrates the sensitive dependence of the classical stabilization on a. As $a \to 0$ and we approach the bare Coulomb potential, S_1 increases rapidly as $1/a^{5/2}$ and the classical dynamics becomes increasingly unstable [30].

Finally we note that although the primary fixed point and secondary fixed points may be unstable there remains an important dynamically invariant, but still unstable, classical structure called the *homoclinic tangle* which appears to play an important role in the quantum theory of stabilization described in Sec. V. The linear stability analysis gives, together with the eigenvalues (25), the corresponding eigenvectors which are straight lines in phase space

$$p = \left[\frac{-S \pm \sqrt{S(4+S)}}{2T}\right] q . \tag{28}$$

When the two eigenvalues are real (and positive, say), then the area-preserving character of the map demands that they be inversely related, i.e., $\lambda_+ = \lambda_-^{-1}$. The eigen-

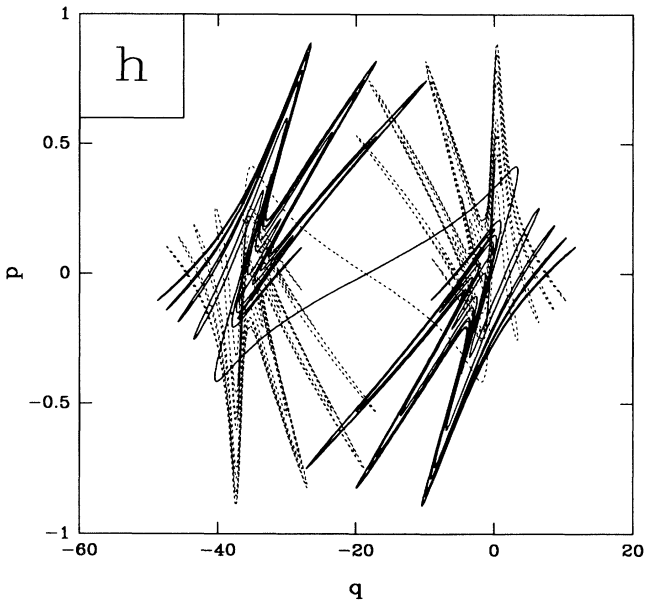

FIG. 6. Homoclinic tangle associated with the fixed point at $(-\alpha, 0)$ for $F = 5.0$ and $\omega = 0.52$. Near the fixed point, the solid line gives the unstable direction while the dashed line is the stable direction. The size of Planck's constant h is shown to illustrate that several states can be supported by the single structure. An estimate of the number of states is given by the number of h boxes needed to cover the structure.

vectors define directions of the Hamiltonian flow towards and away from the fixed point. On leaving the vicinity of the fixed point (beyond which the linear analysis breaks down), these straight-line segments curve and can intersect. Once this happens it can be shown that they intersect infinitely often [10] and the resulting structure is the tangle pictured in Fig. 6 for the SEJ parameters of Fig. 4.

V. QUANTUM ANALYSIS, MAP, AND SCARS

The quantum description of the periodically kicked electron is provided by the quantum map, corresponding to Eq. (14), that is defined by the unitary time-evolution operator for one period of the oscillating field [31]

$$U(T) = \exp(-iTp^2/2)\exp[-V_0(x)]. \tag{29}$$

This quantum KH map provides a very efficient description of the quantum dynamics of an electron in the combined atomic and oscillating fields viewed once every period of the field. By diagonalizing U in a large basis of plane waves using fast fourier transforms we can investigate the structure of the quasienergy wave functions which completely determine the quantum behavior of this periodically perturbed system.

We begin with the case studied by SEJ [7] where the peaks in the stabilized wave function were separated by a distance α. Since the stabilized wave function at

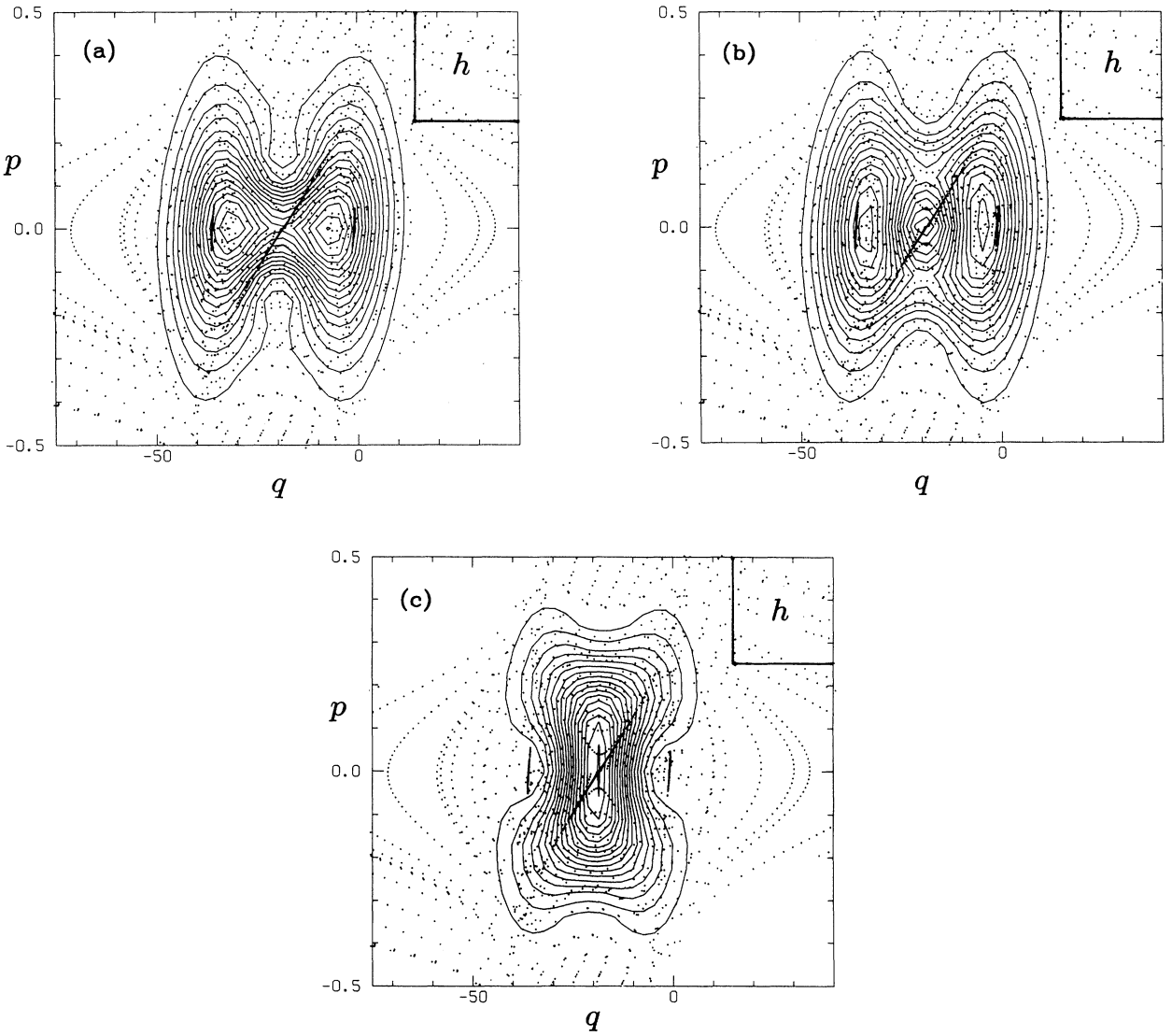

FIG. 7. Level contours of the Husimi distributions of quasienergy states scarred on the (unstable) wells [panels (a) and (b)] and the hyperbolic point (c) of the kicking potential shown in Fig. 1. (a) and (b) show well states of odd and even symmetry, respectively. The classical phase-space trajectories are also shown to correlate the states with the underlying classical invariant structures. The external field parameters are $F = 5$ and $\omega = 0.52$.

peak field will be composed of a superposition of these quasienergy states, this spacing suggests, in close analogy with our previous studies of the microwave ionization of Rydberg atoms [4], that some of these wave functions remain strongly localized to the vicinity of the unstable fixed point at $x = -\alpha_0 = -18.49$ and near the fixed points at $x \approx 0$ and $\approx -2\alpha_0 = -37$.

To check this hypothesis we diagonalized the periodic time-evolution operator in basis of 100 plane waves and found three QE functions that were strongly localized to the vicinity of the classical fixed points. The structure of these quantum wave functions can be conveniently compared with the classical phase space by projecting the QE states onto Gaussian wave packets (coherent states) spanning the classical phase space. (More details of the quantum calculations and the construction of the projections are provided in Appendix B.)

Figure 7 shows the level contours of these so-called Husimi distributions for the quasi energy wave functions superimposed on the classical phase-space trajectories. In Figs. 7(a) and 7(b) are wave functions peaked in the vicinity of the secondary fixed points in the wells of the time-averaged potential near -2α and 0. In configuration space one of these wave functions is odd about $-\alpha$ while the other is even. Figure 7(c) shows a third QE state that is clearly peaked on the unstable fixed point at $-\alpha$. As Planck's constant is large compared with any stable classical structures associated with these periodic orbits all three of these quantum wave functions, which are localized in a chaotic region of the classical phase space, qualify as "scars." In fact, as seen from Fig. 6, the homoclinic tangle in this case is large compared with Planck's constant and provides the most support for the "scarred" wave functions.

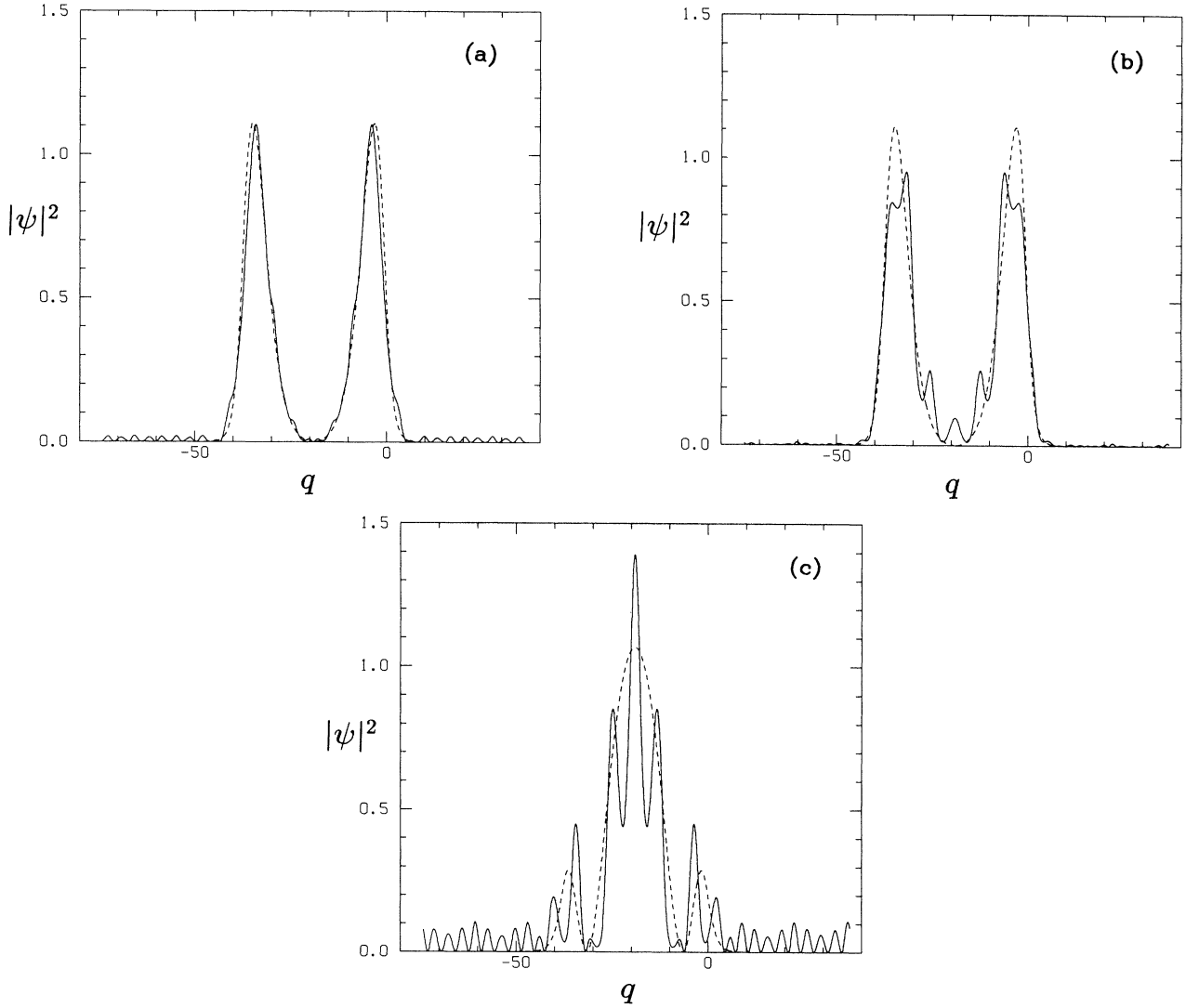

FIG. 8. Coordinate space comparison of quasienergy states (solid lines) with the corresponding eigenstates of the time-averaged KH potential or KH states (dashed lines). As in Fig. 7, (a) and (b) display the odd and even symmetry states associated with the wells while (c) shows a state peaked on the hyperbolic point at $q = -\alpha$. The field parameters are $F = 5$ and $\omega = 0.52$.

Several conclusions can be immediately drawn from this analysis. First, if these QE functions are excited by the application of the strong oscillating field, then some of the electron probability will remain localized to the vicinity of the atom. Second, a superposition of the three QE functions in Fig. 7 will yield a distribution with three peaks spaced α apart. Moreover, a superposition of almost equal amounts of the odd and even states in the wells [Figs. 7(a) and 7(b)] will suppress one of the outside peaks relative to the other by interference leading to a double-peaked wave function with two prominent peaks separated by α. (In fact a close examination of Su's figures [7] reveals a smaller third peak separated by α from the other two.) Third, since the excitation of these wave functions requires the crossing of the classical separatrix (the boundary that separates two distinct types of motion, such as libration and rotation in the case of a simple pendulum) of the double well, they can only be excited diabatically which requires a fast turn-on of the radiation field. The excitation of these localized states and the suppression of the ionization would be greatly diminished by a field that is applied slowly as observed in simulations [7, 12, 15].

As outlined in Appendix B, we can also calculate eigenstates of the KH potential. Figure 8 shows that for the SEJ parameters there are KH eigenstates that show a remarkable resemblance to the quasienergy states whose Husimi distributions were shown earlier. From the coincidence of the peak positions it is clear that the KH states are also well correlated with the classical invariant structures. Although it would be incorrect to conclude that the excited wave function in the time-dependent field is a superposition of the KH states of the time-independent, integrable Hamiltonian, Fig. 8 does indicate that the proper QE states of the time-dependent, nonintegrable Hamiltonian exhibit very similar structure. Why the scarred wave functions of the chaotic systems should have such a strong resemblance to the wave functions of the regular case remains an outstanding open problem for future research.

VI. EXPERIMENTAL IMPLICATIONS

The viability of experimentally observing KH stabilization remains an open question. First, the temporal and spatial features of a "real" laser pulse together with possible effects of a finite bandwidth may preclude the observation. The temporal structure is most crucial to the preparation of the stabilized state and, even within the context of model systems, needs further study. For example, recent 3D numerical simulations suggest that stabilization may be less dependent on turn-on effects in three dimensions than in one dimension [15].

The question of the pulse shape on stabilization is easily addressed within the physical picture we have constructed of the process, that of a free electron interacting with trapping centers. As seen from Eq. (6), a sudden turn-on results in a drift velocity (away from the trapping centers) which is a function of the phase ϕ of the time-dependent field. Stabilization can still occur if the phase of the field is chosen to eliminate this drift. For arbitrary ϕ, this can be achieved by switching on the field over a number of cycles of the external field. The physical mechanism in eliminating the drift is that the *ponderomotive potential* associated with the field gradient is used to compensate for the energy in the drift motion.

This is easily shown for a smooth switching function of the form $\sin^2[\pi t/2\tau_s]$, where τ_s is the time over which the field is being turned-on. As in Sec. II the classical equations of motion can be solved leading to a drift velocity

$$v_d = v_0 - \frac{F}{2\omega}\sin\phi\left(1 - \frac{\omega^2}{(\omega^2 - \pi^2/\tau_s^2)}\right), \tag{30}$$

instead of Eq. (6). It is clear from (30) that when $v_0 = 0$ the drift velocity vanishes for all ϕ provided $\tau_s \gg \tau/2$ where τ is the external period. On considering $\tau_s = s\tau$ this condition becomes $4s^2 \gg 1$, which illustrates clearly why switching over only a few cycles is necessary. The same arguments hold true in the case of any smooth pulse.

Second is the problem of how the high-field stabilization can be detected. The most direct experimental signature would be a measurement of the residual or stabilized atoms. An alternative means of observing the high-field stabilization of electrons is provided by the periodic bremsstrahlung emitted as the stabilized electron scatters off the nucleus each period of the oscillating perturbation. As in the case of harmonic generation (see Ref. [17]), the single-atom emission spectra are obtained from the Fourier transform of a time series of the dipole expectation value. In all cases, the time-dependent dipole expectation value

$$\langle x(t)\rangle = \int x|\Psi(x,t)|^2 dx \tag{31}$$

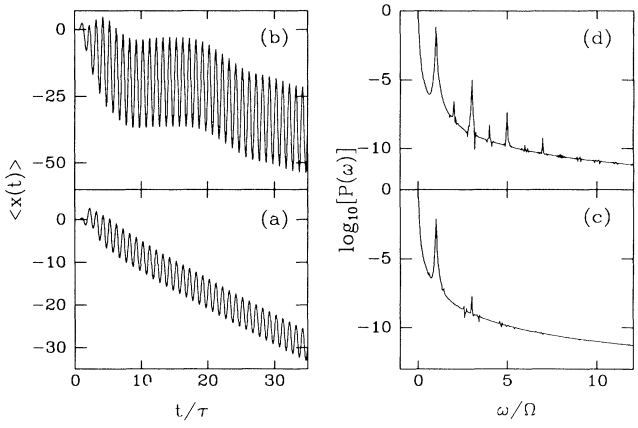

FIG. 9. Time series of dipole expectation values [(a) and (c)] and the associated harmonic generation spectra [(b) and (d)]. The frequency was taken to be 0.52 in all cases. $F = 1.0$ for (a) and (c), which is below the critical field for the onset of stabilization, while for (b) and (d) a higher value $F = 5.0$, where significant stabilization occurs, was considered. The presence of higher harmonics in the spectrum correlates well with increased stabilization.

TABLE I. Conversion efficiencies for harmonics in the stabilized regime contrasted with those for a low-field case. $\Omega = 0.52$ a.u. for all the high-field values and 0.148 for the low-field case. 1 labels the fundamental while Hn represent the nth harmonic. In all cases, the logarithms of the efficiencies are listed.

Field (a.u.)	1	H2	H3	H4	H5	H6	H7	H8	H9
5.0	−1.1	−7.0	−6.7	−8.2	−8.7	−9.2	−9.3	−9.7	−9.8
8.0	−0.9	−7.1	−5.9	−8.2	−8.7	−9.1	−9.3	−9.6	−9.8
10.0	−0.6	−7.2	−5.3	−8.1	−8.5	−9.3	−9.4	−9.8	−10.0
20.0	−0.8	−6.2	−4.7	−8.4	−7.3	−9.1	−8.8	−9.6	−9.9
40.0	−0.8	−5.9	−4.2	−8.3	−6.6	−9.0	−8.4	−9.6	−9.8
0.05	−0.46	−7.8	−1.8	−10.1	−3.3	−10.3	−5.3	−10.9	−7.9
0.06	−0.54	−7.5	−2.2	−9.5	−3.5	−10.1	−5.4	−10.4	−7.4

was constructed using $\Psi(x,t)$ obtained by the direct space-time integration method outlined in Appendix B. For our purposes, it is adequate to define the spectra to be simply the squared modulus of the Fourier amplitudes.

Figure 9 shows the time series and spectra for two values of the field for fixed ω. At the lower field no stabilization has occurred while it has at the higher-field value [32]. The field is switched on smoothly over 5.25τ though the transform is taken only after the peak-field value is reached. In both cases a net drift to one side of the origin is seen, which leads us to anticipate the presence of even harmonics in the emitted light spectrum. Further, in each case, the excursion over a cycle is $\pm\alpha$. In the absence of stabilization, the time series Fig. 9(a) reflects the classical behavior of a drifting oscillating particle. At the lower-field value, the power spectrum in Fig. 9(c) is dominated by the fundamental testifying again to free-particle motion. With increased stabilization at the higher-field value, the free-particle motion is affected by the trapping centers and the time series in Fig. 9(b) shows a retardation of the drift motion. The corresponding power spectrum Fig. 9(d) shows more harmonic structure and the presence of even harmonics in the spectra as well as the absence of a "plateau" of higher harmonics, even at the largest field values. These features distinguish these spectra from those seen at lower, weakly ionizing, field values [17].

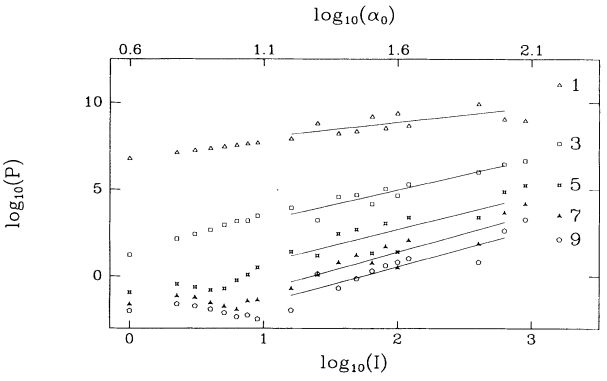

FIG. 10. Intensity (in atomic units) dependence of the power in the fundamental and first four odd harmonics. Unlike the case of low-field harmonic generation, there is no clear intensity dependence and the lines are drawn to guide the eye rather than for any quantitative fit. However, all the higher harmonics are activated at the same value of α which is consistent with the critical intensity for the onset of stabilization. $\omega = 0.52$ for all cases.

For experimental purposes, the conversion efficiency is the most important measure. In particular, as the low-field spectra have been observed, it is interesting to contrast (within the same model) the efficiencies in the stabilized regime with those in typical low-field harmonic spectra. The conversion efficiencies for both even and odd harmonics (the "even" ones being negligibly small) in the low-field case are compared, in Table I, with those in the stabilization regime [33]. Note that the conversion efficiency is defined to be the fraction of the fundamental photon converted into the higher harmonic. Although the conversion efficiencies even at the highest fields are small, the important point is that in the absence of the stabilization there would be no harmonic generation at all.

For the sake of completeness, it should be noted that the power in the odd harmonics, as a function of intensity, shows no distinctive pattern. This is illustrated in Fig. 10 where the power in the fundamental as well as in the first four odd harmonics are shown over a wide range of intensities. The frequency is taken to be 0.52. All the higher harmonics appear to be activated at roughly the same intensity, $\alpha \approx 10$, which is consistent with the critical field strength for the onset of stabilization at this frequency [7, 20]. The lines are drawn to guide the eye to an overall trend of increase though there are significant fluctuations about this trend. This is not surprising considering the number of factors that determine the fraction of the population that is stabilized. This, too, is in marked contrast with the intensity dependence seen in low-field harmonic generation [34].

VII. CONCLUSIONS

We have demonstrated that the language of nonlinear dynamical systems provides a compact and useful description of the phenomenon of atomic stabilization in very intense radiation fields. The key to this analysis

is the construction of a stroboscopic approximation to the full classical dynamics, in the high-field regime. The classical map embodies the realization that the dynamics is specified by more than just the time-averaged behavior. The stability analysis of this mapping based on the computation of classical invariant structures then provides a complete picture of the classical response. Additionally, the quantized version of this map is a good approximation to the full evolution operator over an external period. The quasienergy or Floquet eigenstates of this operator completely specify the quantum response. Thus, the residual stabilized wave function is a superposition of a number of these quasienergy states. The exact composition is decided by the classical invariant structures as well as pulse characteristics. In particular, it is shown that the scarring of some eigenstates on unstable, classical structures is *crucial* to interpreting the structure of the remnant wave function. The application of these ideas to a ground-state atom interacting with optical laser fields may appear to violate traditional intuition which limits the application of classical methods to more obviously "semiclassical" systems, like Rydberg atoms. However, since the stabilized wave function for $\alpha \gg 1$ extends over many atomic units of distance many unperturbed quantum states are strongly coupled, which is precisely the situation where the approximate classical theory is most effective.

ACKNOWLEDGMENTS

We are grateful to P. Bucksbaum, J. E. Eberly, M. Gavrila, R. Grobe, D. Hobson, P. M. Koch, K. Kulander, K. Rzazewski, R. Shakeshaft, R. Scharf, and Q. Su for helpful discussions.

APPENDIX A: DERIVATION OF THE TIME-AVERAGED POTENTIAL AND KICKING TERM

The time-averaged potential is defined to be

$$V_0(q) = \frac{1}{T}\int_0^T V(q - \alpha[\cos(\omega t + \phi) - \cos\phi])dt ,$$

which for the smoothed Coulomb potential and $\phi = 0$ can be written as

$$V_0(q) = \frac{-2}{T}\int_0^{T/2} dt/\sqrt{a^2 + (q + \alpha[\cos\omega t + 1])^2} . \quad \text{(A1)}$$

Let $y = q + \alpha[\cos\omega t + 1]$ which gives

$$dt = \frac{-1}{\omega}\frac{dy}{\alpha\sin\omega t} ,$$

where

$$\alpha\sin\omega t = \sqrt{(r_1 - y)(y - r_2)} ,$$

and $r_1 = q + 2\alpha$ and $r_2 = q$. With these definitions, the time-averaged potential

$$V_0(q) = \frac{-1}{\pi}\int_{r_2}^{r_1}\frac{dy}{\sqrt{(a^2 + y^2)(r_1 - y)(y - r_2)}} ,$$

which, expressed in terms of roots of a quartic, gives

$$V_0(q) = \frac{-1}{\pi}\int_{r_2}^{r_1}\frac{dy}{\sqrt{(y + ia)(y - ia)(r_1 - y)(y - r_2)}} . \quad \text{(A2)}$$

This is evaluated using [35]

$$I = \int_\beta^s \frac{dt}{\sqrt{(\alpha_1 - t)(t - \beta)(t - \gamma)(t - \bar{\gamma})}} = gF(\phi, k) , \quad \text{(A3)}$$

where α_1, β are real; $\gamma, \bar{\gamma}$ are complex; $\alpha_1 \geq s > \beta$ which is satisfied (in our case $\alpha_1 = s$), and where

$$g = \frac{1}{\sqrt{AB}} , \quad k^2 = \frac{(\alpha_1 - \beta)^2 - (A - B)^2}{4AB} ,$$

and (for the case $s = \alpha_1$) $\phi = \pi$,

$$A^2 = (\alpha_1 - b_1)^2 + a_1^2 , \quad B^2 = (\beta - b_1)^2 + a_1^2$$

with

$$b_1 = \frac{\gamma + \bar{\gamma}}{2}$$

and

$$a_1^2 = -\frac{(\gamma - \bar{\gamma})^2}{4} .$$

Using these, we get the value of the integral to be

$$\frac{-1}{\pi}F(\pi, k) \quad \text{(A4)}$$

with

$$g = \frac{1}{\sqrt{(q^2 + a^2)^{1/2}[(q + 2\alpha)^2 + a^2]^{1/2}}} ,$$
$$k^2 = \tfrac{1}{2}\{1 - g^2[a^2 + (q + 2\alpha)q]\} . \quad \text{(A5)}$$

Defining two vectors,

$$\mathbf{r}_- = a\hat{\mathbf{i}} + (q + 2\alpha)\hat{\mathbf{j}},$$
$$\mathbf{r}_+ = a\hat{\mathbf{i}} + q\hat{\mathbf{j}}$$

leads to

$$g = (|\mathbf{r}_+||\mathbf{r}_-|)^{-1/2},$$
$$k^2 = \tfrac{1}{2}\{1 - \mathbf{r}_+.\mathbf{r}_-/(|\mathbf{r}_+||\mathbf{r}_-|)\} .$$

These definitions and the relations

$$F(n\pi \pm \phi, k) = 2nK(k) \pm F(\phi, k)$$

as well as

$$F(0, k) = 0$$

lead to the desired expression [Eq. (20)] for the time-averaged potential.

In deriving the kicking term or impulse, the explicit form

$$V_0(q) = \frac{-2g}{\pi} K(k) \tag{A6}$$

is more appropriate, where g and k^2 are given above. The impulse over one cycle T is given by

$$\Delta p = -\int_0^T \frac{dV_0}{dq} \approx -T \left.\frac{dV_0}{dq}\right|_{\rm TP} ,$$

where TP denotes the turning points of the classical free-particle motion. The derivative of (A6) is

$$-\frac{dV_0}{dq} = \frac{2}{\pi} \left[AK(k) + BE(k) \right] , \tag{A7}$$

where

$$A = \left[\frac{dg}{dq} - \frac{g}{k}\frac{dk}{dq} \right] ,$$

$$B = \frac{g}{k(1-k^2)} \frac{dk}{dq} .$$

It is readily shown that

$$\frac{g}{k}\frac{dk}{dq} = -\frac{g^2}{2k^2}\frac{dg}{dq} \left[a^2 + (q+2\alpha)q \right] - \frac{g^3}{2k^2}(q+\alpha) ,$$

which on using (A5) becomes

$$\frac{g}{k}\frac{dk}{dq} = -\left(\frac{1}{2k^2} - 1 \right) \frac{dg}{dq} - \frac{g^3}{2k^2}(q+\alpha) .$$

Therefore

$$A = \frac{1}{2k^2}\frac{dg}{dq} + \frac{g^3}{2k^2}(q+\alpha)$$

and

$$B = -\frac{(1-2k^2)}{2k^2(1-k^2)}\frac{dg}{dq} - \frac{g^3}{2k^2(1-k^2)}(q+\alpha) ,$$

which can be rewritten as

$$B = -\frac{(k'^2 - k^2)}{2k^2k'^2}\frac{dg}{dq} - \frac{g^3}{2k^2k'^2}(q+\alpha) .$$

As discussed in the text, the turning points are well approximated by $q = 0$ and -2α where $k^2 \approx k'^2 \approx 0.5$. This leads to a simple relation $A = -B/2$ where

$$B \approx -\frac{g^3}{k^2}(q+\alpha) .$$

Therefore, Δp is given by

$$\frac{2BT}{\pi} \left[E(k) - 0.5K(k) \right] , \tag{A8}$$

where this expression has to be evaluated at both turning points. At $q = 0$, the other parameters are

$$g|_{q=0} = \frac{1}{\sqrt{2\alpha}(q^2+a^2)^{1/4}}$$

and

$$k^2|_{q=0} = k_+^2 = \frac{1}{2}\left[1 - \frac{q}{(q^2+a^2)^{1/2}} \right] ,$$

which leads to

$$-\left.\frac{dV_0}{dq}\right|_{q=0} = -\frac{2}{\sqrt{2\alpha}\pi} \frac{[E(k_+) - 0.5K(k_+)]}{(q^2+a^2)^{3/4}} . \tag{A9}$$

Similarly at the other turning point $q = -2\alpha$ we get

$$g|_{q=-2\alpha} = \frac{1}{\sqrt{2\alpha}\left[(q+2\alpha)^2 + a^2\right]^{1/4}}$$

and

$$k^2|_{q=-2\alpha} = k_-^2 = \frac{1}{2}\left[1 + \frac{(q+2\alpha)}{[(q+2\alpha)^2+a^2]^{1/2}} \right] ,$$

which gives

$$-\left.\frac{dV_0}{dq}\right|_{q=-2\alpha} = \frac{2}{\sqrt{2\alpha}\pi} \frac{[E(k_-) - 0.5K(k_-)]}{[(q+2\alpha)^2+a^2]^{3/4}} . \tag{A10}$$

Thus the impulse or kick over a cycle is simply T times the sum of these two contributions which results in (using $\alpha = F/\omega^2$)

$$\Delta p = -\frac{\sqrt{8}}{\sqrt{F}} \left[\frac{[E(k_+) - 0.5K(k_+)]}{(q^2+a^2)^{3/4}} - \frac{[E(k_-) - 0.5K(k_-)]}{[(q+2\alpha)^2+a^2]^{3/4}} \right] . \tag{A11}$$

APPENDIX B: QUANTUM SIMULATIONS

In addressing the quantum dynamics, we considered three distinct approaches.

(i) The first of these is a straightforward space-time integration of the time-dependent Schrödinger equation (in atomic units)

$$i\frac{\partial \Psi(x,t)}{\partial t} = \left[-\frac{1}{2}\frac{\partial^2}{\partial x^2} - V(x) - xE(t) \right] \Psi(x,t) ,$$

using the standard two-sweep algorithm [36]. The parameters of the space-time grid were chosen to optimally ensure both convergence as well as the option to consider reasonably long interaction times. A stringent monitoring of the population reaching the edges of the spatial grid was sufficient to indicate when finite-size effects significantly affected the calculations. The computational procedure was essentially the same as that discussed in Ref. [17] and readers are directed to that work for details.

The one major difference between our calculations and those published earlier is in the measure of ionization. Eberly and co-workers [17] employ the conventional form by projecting out the positive-energy part of the time-dependent wave function. This fraction is then studied as a function of time. Given our picture of the stabilization mechanism as resulting from a free-particle interacting periodically with trapping centers (in this case a double-well potential), we can consider the measure of ionization

to be simply the fraction of wave function that is outside the "interaction volume." As the maximum spacing of the double wells (averaging over an external period) is 4α, a suitable choice for this interaction volume (in one dimension) would be $-4\alpha \leq x \leq 4\alpha$. This definition of ionization as

$$P_I(t) = \int_{|x|>4\alpha} |\Psi(x,t)|^2 dx \tag{B1}$$

is adequate to ascertain when stabilization is significant.

(ii) The second of our three methods employs the map formulation of the classical problem. As shown in Eq. (16), the effective Hamiltonian consists of free-particle motion except for a series of impulses provided by the time-averaged (KH) potential $V_0(\alpha, x)$. As the potential dominates the kinetic term at the kicks, the single period evolution operator is simply expressed as

$$U(T) = e^{-ip^2/2\hbar} e^{-iV_0(\alpha,x)/\hbar} . \tag{B2}$$

This is the corresponding quantum map and it provides a very efficient description of the dynamics. The quasienergy states associated with this operator are then obtained by diagonalizing U within a large basis of plane waves. This amounts to considering a matrix form for U which in the p representation is

$$U_{mn} = e^{-im^2/2} N^{-1} \sum_{j=1}^{N} e^{i(n-m)\theta_j} e^{-iV_0(\alpha,\theta_j)} , \tag{B3}$$

where N is the size of the basis, $\theta_j = 2\pi j/N$, and $\hbar = 1$. The corresponding eigenvalue equation is

$$U(T)|\psi^{(\mu)}\rangle = e^{-i\phi_\mu}|\psi^{(\mu)}\rangle ,$$

where the eigenphases ϕ_μ, $\mu = 1, \ldots, N$ are real. These quasienergy wave functions are sufficient to completely determine the quantum dynamics associated with the map.

The notion of scarring associates individual eigenvectors with invariant structures in the classical phase space. This association is most transparent within a coherent state representation (or "Husimi" distribution [37]) of the individual eigenvectors, that is

$$P^{(\mu)}(q,p) = |\langle q,p|\psi^{(\mu)}\rangle|^2 , \tag{B4}$$

where $|q,p\rangle$ is a coherent state centered at the phase-space point (q,p) and $P^{(\mu)}$ picks up the contribution of $\psi^{(\mu)}$ at that point. The choice of the coherent-state representation is motivated by the symmetries of the classical phase space and here we consider (in p representation) the form

$$\langle n|q,p\rangle = \sum_{l=1}^{N} e^{-[p-(n+lN)]^2/2\sigma} e^{-inq} , \tag{B5}$$

where σ acts as a "squeezing" parameter. This is easily verified from computing the Gaussian distribution corresponding to the Husimi distribution of a coherent state where, for $\sigma = 1$, one recovers the usual minimum uncertainty variances $\Delta q = \Delta p = \sqrt{1/2}$.

(iii) The third of our methods simply diagonalizes the time-averaged potential $V_0(\alpha, x)$ within the same plane-wave basis as the evolution operator, to obtain the KH eigenstates. The procedure outlined above can be used also to construct the Husimi distributions of the KH eigenstates which, in turn, can be correlated with invariant structures in the classical phase space. This is necessary to allow a comparison of the quasienergy and KH states supported by the same classical structure.

* Present address: Department of Physics, Texas A&M University, College Station, TX 77843.

[1] *Irregular Atomic Systems and Quantum Chaos*, edited by J. C. Gay (Gordon and Breach, New York, 1992).
[2] R. V. Jensen, Nature (London) **355**, 311 (1992).
[3] H. Friedrich and D. Wintgen, Phys. Rep. **183**, 37 (1989); D. Delande, in *Chaos and Quantum Physics*, edited by M. -J. Giannoni, A. Voros, and J. Zinn-Justin (Elsevier, London, 1991).
[4] R. V. Jensen, M. M. Sanders, M. Saraceno, and B. Sundaram, Phys. Rev. Lett. **63**, 2771 (1989).
[5] G. S. Ezra, K. Richter, G. Tanner, and D. Wintgen, J. Phys. B **24**, L413 (1991).
[6] R. V. Jensen and B. Sundaram, Phys. Rev. Lett. **65**, 1964 (1990).
[7] Q. Su, J. H. Eberly, and J. Javanainen, Phys. Rev. Lett. **64**, 862 (1990).
[8] M. Pont, N. R. Walet, M. Gavrila, and C. W. McCurdy, Phys. Rev. Lett. **61**, 939 (1988).
[9] H. A. Kramers, *Collected Scientific Papers* (North-Holland, Amsterdam, 1956), p. 866 ; W. C. Henneberger, Phys. Rev. Lett. **21**, 838 (1968).
[10] See, for instance, *Chaos and Integrability in Nonlinear Dynamics: An Introduction*, edited by M. Tabor (Wiley, New York, 1989).
[11] J. I. Gersten and M. H. Mittleman, J. Phys. B **9**, 2561 (1976).
[12] V. C. Reed and K. H. Burnett, Phys. Rev. A **42**, 3154 (1990); V. C. Reed, K. H. Burnett, and P. L. Knight, Phys. Rev. Lett. **61**, 1415 (1991); K. H. Burnett, P. L. Knight, B. R. M. Piraux, and V. C. Reed, *ibid.* **66**, 301 (1991).
[13] M. V. Fedorov and A. M. Movsevian, J. Opt. Soc. Am. B **6**, 928 (1989); M. V. Fedorov and M. Yu. Ivanoff, *ibid.* **7**, 569 (1990).
[14] M. Dörr, R. M. Potvliege, D. Proulx, and R. Shakeshaft, Phys. Rev. A **43**, 3729 (1991).
[15] K. C. Kulander, K. J. Schafer, and J. L. Krause, in *Multiphoton Processes*, edited by G. Mainfray and P. Agostini (CEA, Paris, 1991); Phys. Rev. Lett. **66**, 2601 (1991).
[16] E. J. Heller, Phys. Rev. Lett. **53**, 1515 (1984); in *Chaos and Quantum Physics*, edited by M.-J. Giannoni, A. Voros, and J. Zinn-Justin (Elsevier, Amsterdam, 1991).
[17] J. H. Eberly, J. Javanainen, and K. Rzazewski, Phys. Rep. **204**, 331 (1991).
[18] Also see J. Parker and C. R. Stroud, Jr., Phys. Rev. A

41, 1602 (1990).

[19] R. R. Jones and P. H. Bucksbaum, Phys. Rev. Lett. **67**, 3215 (1991); H. Stapelfeldt, D. G. Papaionnou, L. D. Noordam, and T. F. Gallagher, *ibid.* **67**, 3223 (1991).

[20] R. Grobe and C. K. Law, Phys. Rev. A **44**, R4114 (1991).

[21] J. Grochmalicki, M. Lewenstein, and K. Rzazewski, Phys. Rev. Lett. **66**, 1038 (1991).

[22] L. You, J. Mostowski, and J. Cooper, Phys. Rev. A **45**, 3203 (1992).

[23] See, for example, R. Scharf and B. Sundaram, Phys. Rev. A **43**, 3183 (1991).

[24] The following analysis can be easily extended to other 1D model potentials like $V(x) = -V_0/\cosh^2(|x|/a)$ considered in Ref. [22] and $V(x) = -V_0 e^{-(x^2+b^2)^{1/2}}/\sqrt{a^2+x^2}$ in R. Grobe and M. V. Fedorov, Phys. Rev. Lett. **68**, 2592 (1992). However, the δ-function potentials in T. P. Grozdanov, P. S. Krstič, and M. H. Mittleman, Phys. Lett. A **149**, 144 (1990) and J. Mostowski and J. H. Eberly, J. Opt. Soc. Am. B **8**, 1212 (1991) are too singular.

[25] When the electron experiences the largest interaction with the nucleus on the right side of its oscillatory motion, then the kicks are displaced in time by one half period. In this case, $V_n(q) \approx (-1)^n V_0(q)$, for $q \sim x^-$. For simplicity we will ignore this half-period shift in the timing of the kicks when q crosses the midplane at $-\alpha$. This neglect appears to have little effect on the classical results; however, this additional approximation does appear to complicate detailed comparisons of the approximate quantum map and exact continuous quantum dynamics.

[26] In Ref. [6] the approximate kicking force was defined slightly differently with the field dependence $2\sqrt{2}/\sqrt{F} \equiv k$ factored out of Eq. (23).

[27] The reader should note that the classical electron "surfing" mechanism described by Grobe and Law [20] is simply a recognition of the impulsive interaction of the electron with the nucleus described in detail by our map.

[28] A further test of the validity of the map approximation is provided by a comparison of the Poincaré sections constructed by iterating the map dynamics and by plotting the continuous classical trajectories once every period of the oscillating field. On the scale of Figs. 4 and 5 the structure of the classical phase space in both of these cases would be virtually indistinguishable.

[29] Note that at these parameter values, the fixed points of the map are unstable while the corresponding differential dynamics is only weakly unstable.

[30] T. Mánis, R. Taieb, V. Véniard, and A. Maquet, J. Phys. B **25**, L263 (1992).

[31] S.-J. Chang and K.-J. Shi, Phys. Rev. A **34**, 7 (1986).

[32] As seen, for example, in Fig. 1 in Ref. [7].

[33] It is interesting to note that certain interference effects may lead to nonmonotonic variations in the power seen in the fundamental. These occur due to the mixed character (bound and free) of the stabilized wave function. Both components radiate at the fundamental and the complex Fourier amplitudes can, in principle, interfere giving rise to nonmonotonic variations in the power in the fundamental. This is distinct from low-field harmonic generation where the ionized fraction is small.

[34] K. C. Kulander and B. W. Shore, Phys. Rev. Lett. **62**, 524 (1989).

[35] From P. F. Byrd and M. D. Friedman, *Handbook of Elliptic Integrals for Engineers and Scientists* (Springer-Verlag, Berlin, 1971), p. 133.

[36] S. E. Koonin and D. C. Meredith, *Computational Physics* (Addison-Wesley, Menlo Park, CA, 1990).

[37] K. Husimi, Proc. Phys. Math. Soc. (Jpn.) **22**, 264 (1940).